XVI International Conference on Durability of Building Materials and Components
DBMC 2023, China
K.F. Li and D.P. Fang(Eds)

Durability of GFRP and BFRP Bars in Sulfoaluminate Cement Concrete Made with Seawater and Sea Sand

Tuanjie Wang[1], **Abdul Ghani Razaqpur**[1,2,*]

[1]Sino-Canada Joint R&D Center on Water and Environmental Safety, College of Environmental Science and Engineering, Nankai University, Tianjin 300350, PR China, wtj_lts@qq.com (Tuanjie Wang), Grazaqpur@nankai.edu.cn (Abdul Ghani Razaqpur)

[2]Department of Civil Engineering, McMaster University, Hamilton, Ontario L8S 4L7, Canada, razaqpu@mcmaster.ca (Abdul Ghani Razaqpur)

Abstract. *Due to the large carbon footprint of ordinary Portland cement (OPC) and the rapid corrosion of steel rebars in certain environments, the search for greener, sustainable and more durable reinforced concrete structures is ongoing. In this study, the alkali resistance of basalt- and glass-fibre reinforced polymer (BFRP/GFRP) bars in sulfoaluminate cement (SAC) concrete made with seawater and sea sand is investigated for the first time. Production of SAC involves lower energy consumption and greenhouse gas emission compared to OPC while SAC concrete provides a lower pH environment, which favors the durability of FRP bars. Following ASTM D 7705-D7705M-12 Procedure A, the bars were immersed for three months in simulated pore solution of concrete made with SAC, river sand and fresh water, termed Solution A, and compared their durability to that of companion bars immersed in simulated pore solution of concrete made with SAC, seawater, and sea sand, termed Solution B. Both solutions had the same pH, and their temperature was maintained at 60 ℃ for the duration of the test. The post-immersion or retained tensile strength of GFRP bars in Solution A and B was 83.0% and 73.6%, respectively, while the corresponding values for the BFRP bars were 52.5% and 67.9%, respectively. It appears that due to the presence of sea salt, Solution B is less damaging to BFRP than Solution A while the opposite is true in the case of GFRP. Scanning electron microscopy (SEM) and energy dispersive X-ray spectroscopy (EDS) results are utilized to explain the damage mechanisms. Based on image analysis, it is shown that the deteriorated zone within the bar cross-section is not a uniform ring, but its cross-sectional area correlates with the reduction in tensile strength.*

Keywords: *Durability, FRP Bar, Sulfoaluminate Cement, Seawater, Tensile Strength.*

1 Introduction

It is estimated that cement clinker production contributed 4.0% to global CO_2 emission in 2019 (Olivier, 2022). Compared to Portland cement (PC), calcium sulfoaluminate cement (SAC) is an environmentally more friendly material due to its lower energy consumption and greenhouse gas emission(Alaoui et al., 2007). SAC concrete (SACC) has high early strength, dense pore structure, and good resistance to sulfate attack(Y. Wang et al., 1999), but it has lower pH than the PC concrete (PCC). (Winnefeld and Lothenbach, 2010). Due to its lower pH, it will offer less protection to conventional steel reinforcement, but it offers higher protection to fiber reinforced polymer (FRP) reinforcement because it is less susceptible to attack by low pH in alkaline environments. Consequently, in marine environments, FRP reinforced SACC may be a suitable alternative to conventional reinforced concrete. Furthermore, due to the scarcity of fresh water and river sand in some offshore and near shore regions, SACC made with seawater

and sea sand could be an even more sustainable alternative to conventional reinforced concrete.

To date, many studies have been made regarding the durability of basalt FRP (BFRP) and glass FRP (GFRP) bars made with vinyl ester exposed to simulated pore solution of PC or SAC concrete, made with fresh water and river sand (SACC) or with seawater and sea sand (SW-SACC). However, to the writer's knowledge, no investigation has been conducted regarding the durability of FRP bars made with epoxy resin in SACC or SW-SACC pore solution. Therefore, the objective of the current study is to investigate the durability of GFRP and BFRP bars made with epoxy resin exposed to simulated pore solution of SACC and SW-SACC. Specifically, the effects of exposure temperature and duration on the post-conditioned retained tensile strength and elastic modulus of the bars are investigated. Extensive physiochemical and mechanical tests are performed, and the results are analyzed using modern instruments and techniques to examine the extent and type of changes to the microstructure and chemical composition of the bars constituents and their associated damage mechanisms.

2 Materials and Methods

GFRP and BFRP bars made with epoxy resin, with nominal diameter of 6 mm, Fig. 1, made by different manufacturers, were tested. Table 1 shows their mechanical and physical properties determined as per the relevant specifications of the American Society for Testing and Materials (ASTM).

Table 1. Physical and mechanical properties of control or virgin GFRP and BFRP bars.

Property type	Property	Relevant ASTM standard	GFRP		BFRP	
			Mean Value	COV %	Mean Value	COV %
Physical	Nominal cross-sectional area, mm^2	D792-20	26.60	1.05	27.58	1.09
	Effective bar diameter, mm	D7205/D7205M-21	5.82	0.52	5.93	0.51
	Fiber content, wt%	D2584-18	82.95	0.31	83.16	0.31
	Glass transition temperature, ℃	E1356-08(Reapproved 2014)	104.01	-	104.02	-
Mechanical	Ultimate tensile strength, MPa	D7205/D7205M-21	1223	7.26	1232	5.73
	Tensile modulus of elasticity, GPa	D7205/D7205M-21	53.42	1.91	50.51	3.16

Two kinds of conditioning solutions were used in this study. The PS solution was designed to simulate the pore solution of SACC made with fresh water and river sand, whose chemical composition was based on the data provided in (L. Wang et al., 2019). The SS solution was designed to represent the pore solution of SACC made with seawater and sea sand. It was made by modifying the PS solution composition with the addition of simulated seawater. As shown in Table 2, both solutions had pH of 12.9 at 25℃.

Sets of bars were immersed in the two solutions under constant 60 ℃ for 30, 60 and 90 days, and after each of these exposure periods were drawn and tested to determine their retained tensile strength and elastic modulus. In each case, at least five replicate specimens were tested as per ASTM D7205 specifications.

Table 2. Chemical compositions of simulated pore solutions in this study.

Type	Quantities (gram per liter)						pH
	KOH	$NaAlO_2$	K_2SO_4	NaCl	Na_2SO_4	KCl	
PS	1.403	9.017	9.584	-	-	-	12.9
SS	2.132	9.017	9.584	32.136	4.09	0.695	12.9

In the BFRP bars, the part of the conditioned bars cross-section permeated by the solution could be seen by the naked eye; hence, a camera was used to capture digital images of the permeated or stained cross-sections. The images were analyzed by Fiji software to determine the precise area of the stained part of each cross-section. Pre- and post-conditioned cross-sections of bars were also examined by Scanning Electron Microscopy (SEM) and Energy-dispersive X-ray Spectroscopy (EDS) to track to their microstructure and chemical composition due exposure to the solutions.

3 Results and Discussion

3.1 Retained Tensile Strength and Elastic Modulus

Fig. 1 (a) and (b) shows the effect of exposure solution and duration on the retained tensile strength and elastic modulus of the the two types of bars conditioned at 60 ^oC. Specimens are designated as FST6D#, where F represents fiber type, B for basalt and G for glass, S represents the type of solution, PS or SS, T60 exposure temperature in ^oC, and D# number of exposure days (30, 60 or 90). GR and BR represent the the reference GFRP and BFRP bars, respectively.

Exposure duration longer than 30 days resulted in dramatic reduction in strength. After 90 days of immersion in the PS and SS solutions, the tensile strength of the GFRP bar dropped by 17% and 26%, respectively, while that of the companion BFRP bar dropped by 47.5% and 32% , respectively. Note, while the addition of seawater to the PS solution reduced the durability of the GFRP compared to the pure PS solution, on the contrary, it bolstered the durability of the BFRP. Based on these results, BFRP may experience severe damage in conventional SACC made with fresh water while in SW-SACC, it will perform better.

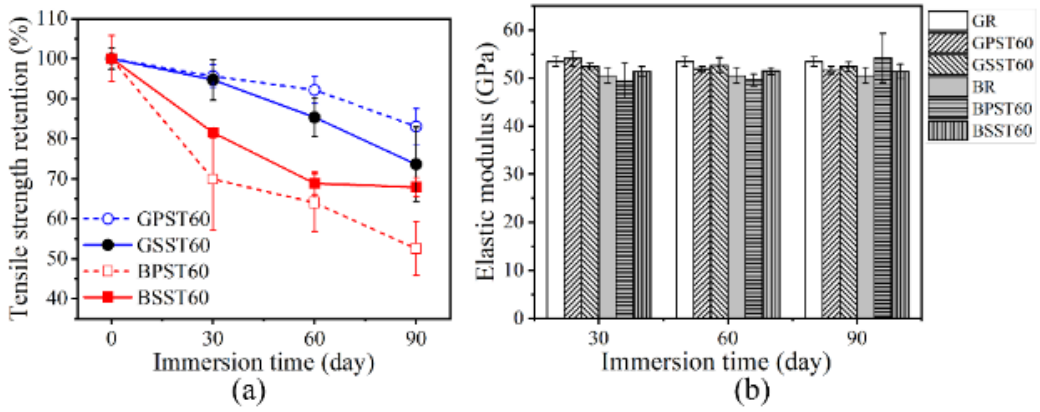

Fig. 1. Conditioned bars (a) Retained tensile strength, (b) Elastic modulus.

Fig. 1 (b), shows that none of the exposure conditions had practically significant effect on the elastic modulus of either type of bar. Since the elastic modulus is calculated as the slope of the bar stress-strain curve at low strain levels (between 0.001 and 0.003), it means that for practical purposes, stress-strain characteristic was not significantly affected at such strain levels.

3.2 Bar Cross-section Staining

Fig. 2 shows the typical progression of the stain in the BFRP bars immersed in the SS solution. A similar phenomenon was also reported in (Katsuki and Uomoto, 1995). It should be mentioned that the outermost ring in each image is a new coat of epoxy applied after conditioning to protect the outer surface of the bars from damage during saw cutting.

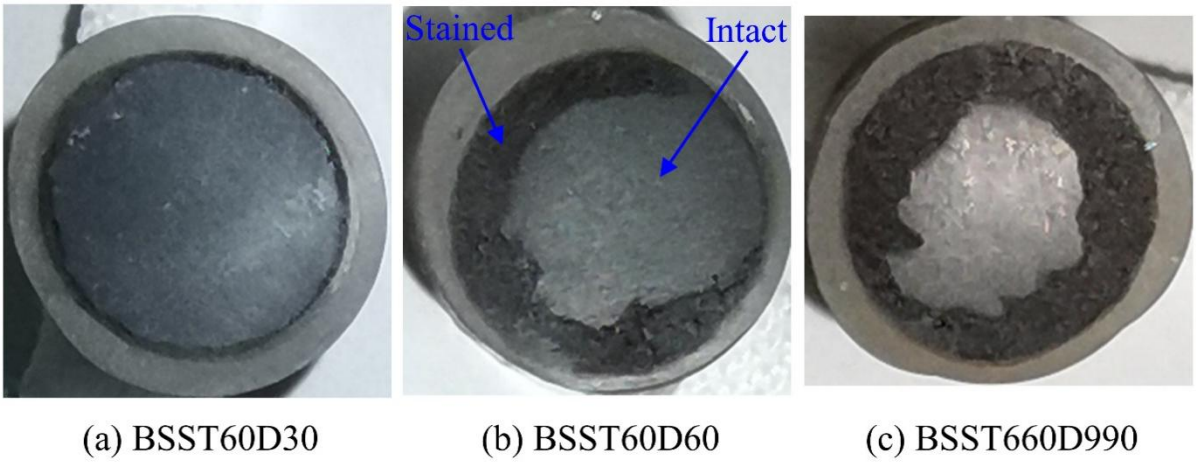

Fig. 2. Typical stained cross-section of the conditioned BFRP bars.

It is proposed here that for immersion in a solution for a period *t* (days), the relationship between the % retained strength and % intact (unstained) area of the bar cross-section can be expressed as

$$S(t) = K\ Log\left(\frac{A_I}{A_o} \times 100\right) \tag{1}$$

where *S (t)* = % of initial tensile strength retained at time *t*, *K*= a parameter to be determined experimentally and is termed as the calibration factor, A_I = area of intact part of the bar cross-section, A_o = initial cross-sectional area of the bar.

The applicability of this relationship to the data in Table 3 is checked as follows. For the bars immersed in the two solutions, their experimentally measured $\frac{A_I}{A_o}$ and *S(t)* values for 30 days are inserted in Eq.(1) to determine the relevant *K* values. This gives *K* equal to 36.77 and 42. 42 for the bars immersed in the PS and SS solution, respectively. Using these *K* values in Eq.(1), the *S(t)* values for the bars immersed in each solution for 60 and 90 days are computed and designated as S_p, as in Column 6 of Table 3, while Column 7 gives the ratio of the computed to the experimentally measured retained tensile strength, S_T. The ratios in the last column show for all the bars remarkably good agreement between the computed and measured strengths.

Table 3. Predicted % tensile strength based on image analysis.

Specimen	% Unstained area measured		% Strength retained based on tension test, S_T		% Strength retained as predicted by Eq. (1), S_p	$\frac{S_P}{S_T}$
	Mean	COV (%)	Mean	COV (%)		
BPST60D30	79.6	8.6	69.9	18.26	69.9	1.00[(a)]
BPST60D60	50.6	11.3	64.0	11.30	62.7	0.98
BPST60D90	25.2	13.3	52.5	12.78	51.6	0.98
BSST60D30	83.4	4.6	81.5	1.50	81.5	1.00[(a)]
BSST60D60	57.3	4.2	68.8	4.15	74.6	1.08
BSST60D90	38.3	15.2	67.9	3.53	66.8	0.98

(a): The S_T value of this specimen was used to determine the relevant calibration factor for each solution.

3.3 SEM-EDS Analysis

Typical pre- and post-immersion SEM images of the test bars cross-sections are shown in Fig. 3. Fig. 3 (a) and (b) shows in the reference GR bar microcracks at the fiber-matrix interface and within the matrix in certain zones. After 30 days of immersion in the SS solution, new cracks joined the existing ones as in Fig. 3 (e), and the existing defects connect through fiber-matrix interface. After 90 days, the initially cracked zones turned into pits or tiny cavities (see Fig. 3 (f)). Additionally, white circular lines - possibly deposited by the solution -, became visible at some fiber-resin interfaces as well as erosion of the cross section of some fibers. It may be conjectured that some of these defects were caused by samples preparation, but the same method was used to prepare all the samples, so it is unlikely that the observed damages were caused by the sample preparation. As evidence, such defects are not visible in the top left corner in Fig. 3 (g), while they are visible in most of the other zones in the same figure.

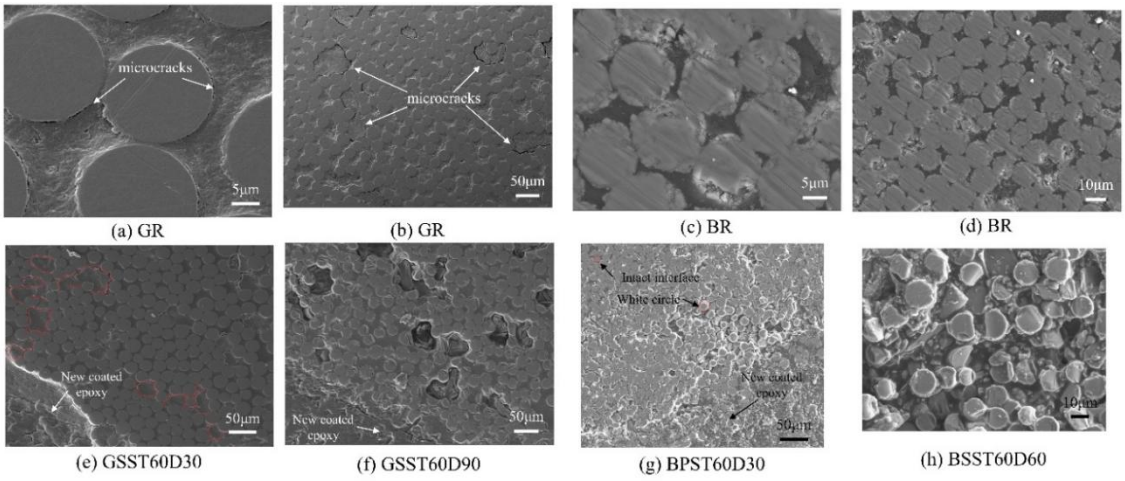

Fig. 3. Typical SEM images of pre-conditioned (a-d) and post-conditioned (e-h)test bars.

Similarly, white circular lines formed at the interface of some basalt fibers in the BFRP bars as can be seen in image (g) of Fig. 3. Fig. 3 (h) shows severe erosion of fibers in specimen BSST60D60. Compared to the GFPR specimens, the white circles in the BFRP specimens formed much earlier and their density was higher. These line may indicate the damage to the sizing of the fibers or could be corrosion shells. Corrosion shells in SEM micrographs have been reported in conditioned FRP composites by others (Guo et al., 2018).

The EDS analysis results for the fibers and the matrix of each type of bar pre- and post-conditioning are summarized in Table 4. The locations of points probed in the post-conditioned bars cross-sections are shown in the relevant SEM micrographs in Fig. 4. The results in Table 4 indicate that Si (rather SiO_2) is the dominant oxide in both GR and BR, having similar wt% in the two types of fibers, but the wt% of calcium (Ca) and zirconium (Zr) in GR are significantly larger than those in BR. On the other hand, the Na, Mg, K and Fe contents of BR are significantly larger than those of GR. Based on X-ray Photoelectron Spectroscopy (XPS) analysis of the present basalt fiber powder, the atomic ratio of Fe^{2+} to Fe^{3+} was found to be approximately 1:3.

The high iron content of basalt fibers is responsible for their dark brown color (M. Wang et al., 2008). It is well known that high alkali oxide content in glass and basalt fibers will reduce the fiber durability in solutions while the high zirconium and calcium oxide contents will improve it(Nkurunziza et al., 2005). Also, as reported in (Halder et al., 2016), the presence of high zirconium in the fiber will enhance its bonding to the epoxy. It can be also observed that the matrix in the GFRP bar has much higher zirconium content than that in the BFRP bar.

For specimen GPST60D90, point GF1 in Fig. 4(a) is located near the periphery of the damaged fiber. At this point, with reference to the data in Table 4, compared with the virgin glass fiber in GR, the Si and Ca contents are significantly smaller while the Na, K, and Mg contents are slightly less. The reduction in the silica content indicates the dissolution of silica from the fiber into the matrix. Point GM1 is in the damaged matrix adjoining a glass fiber, where the Si content is significantly greater while the Na, K, and Mg contents are somewhat larger compared to those in the GR matrix. The increase in the Si content of the matrix can be attributed to the dissolution of the silicate in the adjoining fiber.

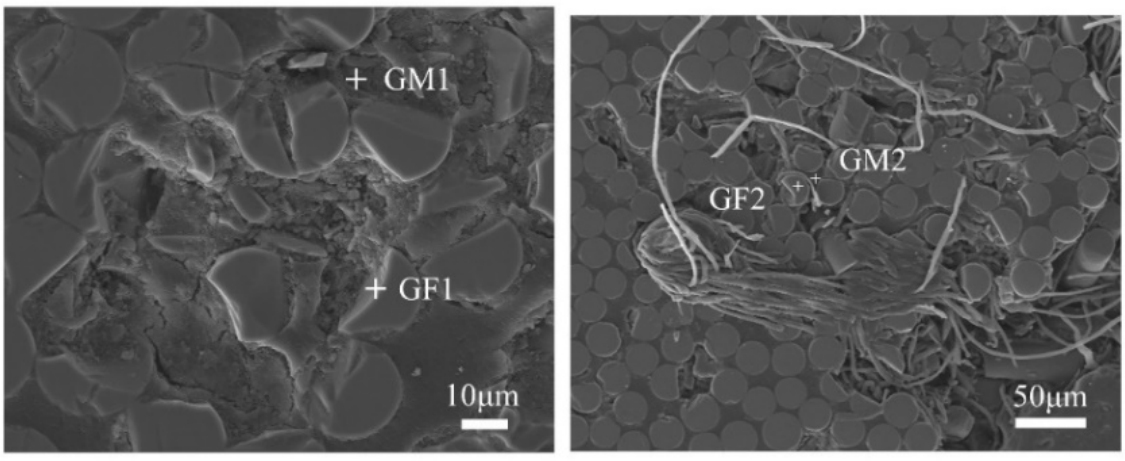

(a) GPST60D90 (b) GSST60D90

Fig. 4. Location of points selected for SEM-EDS probing in the conditioned FRP bars.

Table 4. EDS test results of typical BFRP and GFRP specimens pre- and post- exposure to solutions.

Specimen	Spect-rum	wt% percent of chemical elements present in each bar													
		C	O	Na	Mg	Al	Si	S	Cl	K	Ca	Ti	Fe	Zr	Total
GR		2.29	37.41	0.36	1.54	6.87	27.63	0.22	0.03	0.24	15.95	0.21	0.18	7.05	99.98
GR		68.08	15.64	0.10	0.27	0.32	1.48	0.66	0.46	0.00	0.94	0.04	0.22	11.79	100.00
GPST60D90	GF1	28.18	28.26	0.31	0.95	4.52	18.45	0.26	0.04	0.20	11.28	0.17	0.23	7.15	100.00
GPST60D90	GM1	40.02	16.52	0.3	0.52	2.70	12.65	1.89	0.60	0.71	11.49	0.22	0.97	11.42	100.01
GSST60D90	GF2	4.84	36.74	0.37	1.53	6.63	26.48	0.18	0.06	0.25	15.63	0.25	0.18	6.86	100.00
GSST60D90	GM2	68.01	7.59	0.34	0.13	0.60	1.80	1.24	0.76	0.34	1.83	0.05	0.07	17.24	100.00
GSST60D90	GF2	4.84	36.74	0.37	1.53	6.63	26.48	0.18	0.06	0.25	15.63	0.25	0.18	6.86	100.00
BR		2.78	41.11	2.37	3.92	7.65	24.66	0.00	0.03	4.11	4.10	1.59	5.55	2.14	100.01
BR		71.56	20.59	0.20	0.21	0.36	1.16	0.09	0.29	0.19	0.25	0.16	0.44	4.52	100.02

With reference to Fig. 4 (b), in the GSST60D90 specimen, the selected point, designated as GM2, is in the damaged matrix, where, as shown in Table 4, some increase in the Si, Na, K and Ca contents can be noticed compared to the those in the virgin matrix. The increase can be attributed to the dissolution of these species from the fiber. This can be corroborated by considering point GF2, located at the center of a damaged fiber in the last specimen, where practically no change in the Si, Na, Mg, and K contents can be noticed compared to corresponding contents in the companion virgin fiber because the fiber center was not in contact with the solution.

4 Conclusions

This investigation supports the following conclusions:

- Both GFRP and BFRP experienced significant damage after 90 days of immersion in both solutions, but the BFRP experienced 279% and 123% more damage than the GFRP in the PS and SS solution, respectively.
- The GFRP experienced 153% more damage in the SS solution than in the PS solution while the BFRP experienced 33% less damage in the SS solution than in the PS solution. Hence, the seawater had beneficial effect on the durability of the BFRP while it had deleterious effect on that of GFRP.
- The part of the BFRP bars cross-sections stained by the permeated solution was visible to the naked eye. The area of this part correlated well with the reduction in the tensile strength of the bar. A proposed equation accurately captured the relation between the two.
- Detailed SEM examination and EDS chemical analysis revealed that both the matrix and the fiber suffered damage as result of immersion in either solution, but the BFRP fibers suffered more damage due their dissolution in the diffused solution.

Acknowledgements

This work was supported by research grants from the Foreign Expert High Level Talent Program, the Ministry of Science and Technology of China, the Haihe Talent Special Project and the Tianjin Municipal Government, which are gratefully acknowledged.

ORCID

Tuanjie Wang: https://orcid.org/0000-0003-0768-9851
Abdul Ghani Razaqpur: https://orcid.org/0000-0002-9529-064X

References

Alaoui, A., Feraille, A., Steckmeyer, A., and Roy, R. L. (2007). *New Cements for Sustainable Development*. Proceedings of 12th International Congress on the Chemistry of Cement, Montreal (CA).

Guo, F., Al-Saadi, S., Raman, R. K. S., and Zhao, X. L. (2018). *Durability of fiber reinforced polymer (FRP) in simulated seawater sea sand concrete (SWSSC) environment*. Corrosion Science, 141, 1–13. https://doi.org/10.1016/j.corsci.2018.06.022

Halder, S., Ahemad, S., Das, S., and Wang, J. (2016). *Epoxy/Glass Fiber Laminated Composites Integrated with Amino Functionalized ZrO_2 for Advanced Structural Applications*. ACS Applied Materials & Interfaces, 8(3), 1695–1706. https://doi.org/10.1021/acsami.5b09149

Katsuki, F., and Uomoto, T. (1995). *Prediction of deterioration of FRP rods due to alkali attack*. Non-Metallic (FRP) Reinforcement for Concrete Structures, 29, 82–89.

Nkurunziza, G., Debaiky, A., Cousin, P., and Benmokrane, B. (2005). *Durability of GFRP bars: A critical review of the literature*. Progress in Structural Engineering and Materials, 7(4), 194–209. https://doi.org/10.1002/pse.205

Olivier, J. G. J. (2022). *Trends in global CO_2 and total greenhouse gas emissions: 2021 Summary Report* (PBL publication number: 4758). PBL Netherlands Environmental Assessment Agency.

Wang, L., Zhan, S., Tang, X., Xu, Q., and Qian, K. (2019). *Pore Solution Chemistry of Calcium Sulfoaluminate Cement and Its Effects on Steel Passivation*. Applied Sciences-Basel, 9(6), 1092. https://doi.org/10.3390/app9061092

Wang, M., Zhang, Z., Li, Y., Li, M., and Sun, Z. (2008). *Chemical Durability and Mechanical Properties of Alkali-proof Basalt Fiber and its Reinforced Epoxy Composites*. Journal of Reinforced Plastics and Composites, 27(4), 393–407. https://doi.org/10.1177/0731684407084119

Wang, Y., Su, M., and Zhang, L. (1999). S*ulphoaluminate Cement (in Chinese)* (1st ed.). Beijing University of Technology Press.

Winnefeld, F., and Lothenbach, B. (2010). *Hydration of calcium sulfoaluminate cements—Experimental findings and thermodynamic modelling*. Cement and Concrete Research, 40(8), 1239–1247. https://doi.org/10.1016/j.cemconres.2009.08.014